ICARUS **129,** 450–465 (1997)
ARTICLE NO. IS975793

Simulations of the Atmospheres of Synchronously Rotating Terrestrial Planets Orbiting M Dwarfs: Conditions for Atmospheric Collapse and the Implications for Habitability

M. M. Joshi, R. M. Haberle, and R. T. Reynolds

Space Sciences Division, NASA Ames Research Center, MS 245-3, Moffett Field, California 94035–1000
E-mail: joshi@humbabe.arc.nasa.gov

Received April 11, 1997; revised June 9, 1997

Planets within the habitable zones of M dwarfs are likely to be synchronous rotators; in other words, one side is permanently illuminated while the other side is in perpetual darkness. We present results of three-dimensional simulations of the atmospheres of such planets, and comment on their possible habitability. Near the ground, a thermally direct longitudinal cell exists, transporting heat from the dayside to the nightside. The circulation is three-dimensional, with low-level winds returning mass to the dayside across the polar regions. Aloft, the zonally averaged winds display a pattern of strong superrotation due to these planets' finite (albeit small) rotation rate. With terrestrial values of insolation, a CO_2/H_2O atmosphere collapses, or condenses on the surface of the darkside, when surface pressure is approximately 30 mb, this value being much lower for a N_2 atmosphere. This temperature contrast is also sensitive to factors such as gravity, planetary radius, and IR optical depth τ. These results question the suitability of the concept of a habitable zone around M dwarfs that is independent of planetary parameters. If CO_2 partial pressure is controlled by the carbonate–silicate cycle, we find that these planets should have a minimum surface pressure of 1000–1500 mb of CO_2, as this is the minimum pressure needed to support stable liquid water on the darkside at the inner edge of the habitable zone. We finally conclude that planets orbiting M stars can support atmospheres over a large range of conditions and, despite constraints such as stellar activity, are very likely to be habitable. © 1997 Academic Press

INTRODUCTION

The habitable zone around the star is a range of orbital distances (and hence stellar luminosities) in which a planet is most likely to be able to support life. There are many definitions for such a locus, but one common one is defined by the range in which a planet can support liquid water somewhere on its surface (Kasting *et al.* 1993).

M stars constitute approximately 75% of the stellar population (Rodonò 1986) but are the smallest and least luminous of main sequence stars, having masses 0.1–0.5 times the mass of the Sun. The habitable zones around such stars are therefore very close, being typically between 0.03 and 0.4 AU [see Fig. 16 of Kasting *et al.* (1993)]. A planet lying this close to its star will tend to become tidally locked, or in other words be permanently illuminated on one side, as the threshold for tidal locking after 4.5 byr is $r_{\rm lock} \approx 0.5(M_{\rm star}/M_{\rm sun})^{1/3}$ [see Fig. 16 of Kasting *et al.* (1993) and Dole (1964)]. Such planets are termed synchronous rotators, and their rotation rates are therefore governed by the size of their orbits (this is dealt with below).

If the atmosphere of such a planet is in radiative–convective equilibrium, the surface temperature T_0 on the dayside will be very high, while the nightside will be so cold that the major atmospheric constituent will condense out on the surface. When this happens, the surface temperature of the darkside, as well as the mean surface pressure p_0, is set by a balance between upwelling thermal radiation and release of latent heat by condensing constituents, similar to the scenario that has been postulated for the martian atmosphere at those times when a permanent polar cap forms (see, e.g., Toon *et al.* 1980). In this latter case, surface pressures have been modeled as being as low as 1–3 mb (Toon *et al.* 1980). This phenomenon is termed atmospheric collapse, and has been put forward as the primary reason against searching for habitable planets around M stars.

In reality, atmospheric motions reduce the day/night temperature gradient $\Delta T_{\rm DN}$ by transporting heat. Simplistically, it can be seen that the higher the atmospheric mass, the more horizontal atmospheric motions (hereafter referred to as advection) should dominate over radiation. This can be restated as advection will become important when the advective time scale becomes small enough to be comparable to the radiative relaxation time scale.

The advective time scale $t_{\rm d}$ is simply $\Delta L/U$, where ΔL is the day–night distance, and U is a typical atmospheric windspeed. From Goody and Yung (1989), the radiative relaxation time scale of a planetary atmosphere for global scale motions $t_{\rm r}$ is given by

0019-1035/97 $25.00

$$t_r = c_p p_0 / \sigma g T_e^3, \quad (1)$$

where c_p is the specific heat of the gas, σ is the Stefan–Boltzmann constant, T_e is the effective emission temperature of the planet, and p_0 is surface pressure. This time scale is most dependent on p_0, as this parameter can vary over many orders of magnitude. It will also depend on the planet's size through the dependency on g. The substellar–antistellar surface temperature difference ΔT_{DN} is then determined by the relative values of t_r and t_d.

As an example, setting terrestrial values for c_p, g, p_0, and ΔL, and assuming $T_e = 250$ K and $U = 10$ msec^{-1}, $t_r = 160$ days, while $t_d = 20$ days, which indicates that even for an Earth-like planet, horizontal advection is strong enough to move the darkside away from radiative equilibrium and prevent atmospheric collapse. This scale analysis, while being simple, does demonstrate that ΔT_{DN}, and hence the ability of synchronously rotating planets to support atmospheres, is sensitive to a wide variety of planetary and atmospheric parameters.

Haberle *et al.* (1996) used a simple energy balance model to show that a pure CO_2 atmosphere having a value of p_0 of about 150 mb was sufficiently dense to allow the darkside of such a planet to warm up to above the freezing point of CO_2. They accounted for heat transport by a simple formulation which was proportional to p_0 and quadratic in ΔT_{DN}. This model showed that even for relatively low atmospheric pressures, atmospheric transport of heat to the nightside could counteract the effect of radiative cooling. While this model has produced some encouraging results, it must be emphasized that it is a very simple model and that all the aspects of the atmospheric circulation are folded into just one parameter. A global circulation model is needed to better characterize the ability of such planets to support atmospheres.

Initial work by Joshi and Haberle (1996) showed that 100 mb of CO_2 was sufficient to support an atmosphere on an Earth-sized planet. We now present more detailed results from this investigation. The model is described, and the range of parameters used in the experiment explained. The circulation of the atmospheres of these planets is presented. The sensitivity of T_0 and ΔT_{DN} to factors such as pressure, optical depth, and planetary radius is examined in the context of under what conditions atmospheric collapse may occur. We then investigate sources of transience in these atmospheres, both internally forced (i.e., atmospheric waves) and externally forced (i.e., by starspots). We finally discuss the results in the context of the habitability of planets orbiting M stars.

MODEL DESCRIPTION

The model used is a modified version of the so-called SGCM or simplified global circulation model (Joshi *et al.* 1995, James and Gray 1986). The SGCM can be thought of as consisting of two parts: an adiabatic (or transport) part, and a diabatic (or radiation and friction) part. Model variables are represented by spherical harmonics truncated at a specified wavenumber. The model employs the σ coordinate system in the vertical, where σ denotes pressure/surface pressure. The adiabatic part solves the primitive equations of dynamical meteorology on the sphere (Hoskins and Simmons 1975, Holton 1992).

At this point we emphasize that the SGCM represents terrestrial-type planets, or those planets consisting of a relatively shallow atmosphere covering a thick rocky planet. The assumptions made in formulating the primitive equations of motion used in the model are not strictly applicable to large gaseous planets like Saturn and Jupiter.

The radiative scheme in the model consists of a simple representation of solar heating of the surface, where the solar flux is given by

$$F = F_0 \cos\phi \cos\lambda \quad (-\pi/2 \geq \lambda \geq \pi/2), \quad (2)$$

$$F = 0 \quad \text{elsewhere}, \quad (3)$$

where ϕ is latitude and λ is longitude. The IR part of the radiation is now handled by a simple two-stream gray approximation (rather than Newtonian relaxation, as was the case previously). Exchanges of heat and momentum between the surface and atmosphere are handled by a quadratic formulation, detailed in Eqs. (7)–(9) of Joshi *et al.* (1995). Heat is mixed uniformly in convectively unstable regions.

The surface energy balance is very important, as this determines the surface temperature T_0. This is simply a balance between downwelling solar insolation F_D, upwelling IR radiation (black body radiation), downwelling IR radiation F_G (the greenhouse effect), and sensible heat fluxes between atmosphere and ground F_S. The expression for the time evolution of T_0 is

$$\alpha \partial T_0 / \partial t = (1 - a) F_D + F_G - F_S - \sigma T_0^4 + L, \quad (4)$$

where a is the ground albedo, and L is the latent heat released by condensing CO_2. The factor α represents the thermal inertia of the ground. The higher the thermal inertia, the more heat is dissipated into the ground via conduction. This time scale was set to 10^5 sec, which suppressed instabilities in T_0 and yet meant that T_0 was able to respond effectively to transient forcing by mechanisms having periods longer than 1 day (see below).

The condensation of CO_2 was modeled by not allowing the surface or atmosphere to fall below its frost point. This was done by an energy conservation scheme that condensed sufficient CO_2 such that the amount of heat energy gained equaled the latent heat energy released by

condensation. The surface pressure was then adjusted at the appropriate grid points, and the surface albedo changed to that of ice. The frost point of CO_2 varies a great deal with pressure (Kasting 1991). For this work, the frost point was approximated by the relation

$$T_{\text{cond}} = 194.5 + 27.75P + 3P^2, \quad (5)$$

where P is in bars. If CO_2 condensation on the ground occurred, this was deemed as an indication that the atmosphere was collapsing (as the nightside frost was permanent) and that the atmosphere was falling into another regime where T_0, P_0, and ΔT_{DN} were controlled by CO_2 ice (Haberle *et al.* 1996). The model conditions under which such collapse happened were then noted.

Model Parameters

The nominal simulations used terrestrial values for radius, gravity, gas constant, and stellar insolation S (hereby defined as S = insolation/terrestrial insolation = 1 in the nominal runs).

The ground albedo in all the runs was set to 0.2, consistent with earlier simpler one-dimensional calculations. The reason for this low value is the decreased importance of Rayleigh scattering due to the low emission temperature of M dwarfs (Kasting *et al.* 1993). This value is slightly lower than the value of 0.3 used in the initial three-dimensional calculations (Joshi and Haberle 1996).

For the nominal runs, the radiation scheme was tuned such that IR optical depth $\tau = 0.3$ when $p_0 = 100$ mb, $\tau = 1.0$ when $p_0 = 1000$ mb (similar to that of Earth), and $\tau = 1.5$ when $p_0 = 1500$ mb. These values are equal to that expected from a pure CO_2 atmosphere (Pollack *et al.* 1987), but are also similar to that of the Earth ($\tau_{\text{Earth}} \approx 0.9$). Atmospheres having very different compositions (e.g., N_2/CH_4) would be expected to have very different IR optical depths for similar surface pressures. This effect was examined by studying the effect of varying τ at a given value of p_0.

The momentum balance on slowly rotating planets, and hence the mean wind field, is thought to be determined largely by momentum transports by the mean circulation as well as large-scale eddies having zonal wavenumbers 1–2 (Del Genio *et al.* 1993). However, previous simulations of Titan have shown that resolution higher than 32 points in longitude may be necessary to adequately simulate the high winds there (Hourdin *et al.* 1995). Windspeeds will also depend on internal dissipation and drag, which are completely unknown here.

All model runs were carried out at so-called T10L10 resolution, which means truncation in the horizontal at maximum total horizontal wavenumber 10 (equivalent to having 32 grid points in longitude), and 10 layers in the vertical equispaced in σ or p/p_0. This was justified by the fact that the standard 1-bar run repeated at T21 resolution produced surface temperatures similar to the T10 case to within 5 K.

The rotation rate was determined by assuming that for a synchronous rotator, the rotation rate is the same as the orbital period. For a star of 0.1 solar mass, the orbital radius R is 0.02–0.03 AU, and the angular frequency ω (or $2\pi/P$) is approximately 10^{-5} sec^{-1}. For a star of 0.5 solar mass, R = 0.2–0.3 AU and $\omega \approx 10^{-6}$ sec^{-1}.

This is an important result as a planet having a low rotation rate might exhibit the same sort of circulation as Titan, with mean meridional cells extending to the midlatitudes and strong prograde jets at high latitudes (Hourdin *et al.* 1995). Atmospheric waves forced by topography and thermal effects can also contribute to prograde jets forming at lower latitudes, as is the case on Venus (Pechmann and Ingersoll 1984).

All of the nominal experiments were done using a rotation rate similar to that of Titan (4.5×10^{-6} sec^{-1}), as it was found that the circulation was relatively insensitive to the rotation rate, due to the strength of the thermal forcing due to the synchronous heating (see later). The nominal runs were integrated forward until the zonal wind at the equator had equilibrated to a constant value and the momentum balance had reached a (statistically) steady state. The time scale for this was 100 Titan days (about 1620 Earth days). It was also noted that the surface temperature equilibrated within 20–30 Titan days in the nominal runs.

ATMOSPHERIC CIRCULATION IN THE SGCM

Simulations with Zonally Averaged Heating

As a prelude to the full results which incorporate the effect of synchronous heating, we present results from a model run with zonally averaged heating (i.e., F is independent of longitude). This will demonstrate the ability of the model to reproduce results of studies done with terrestrial GCMs having low rotation rates (Del Genio *et al.* 1993). P_0 and τ were set to 1000 mb and 1.0, respectively. To closely match the results of Del Genio *et al.*, a representation of stratospheric drag was introduced in the control run in the form of Rayleigh friction with a time scale of 0.5 Titan day in the topmost layer (only in this control run).

Zonal-mean cross sections of the temperature and wind fields are shown in Fig. 1. It can be seen that the zonal (W–E) wind exhibits a pattern of slight westerlies over the equator and westerly jets in near the poles. The presence of the equatorial westerlies is a result of non-axisymmetric eddies (Hide 1969), and their strength is dependent on factors such as atmospheric stability at the equator and rotation rate. The equatorial westerlies in fact appear slightly stronger in this run than in Del Genio *et al.* (1993).

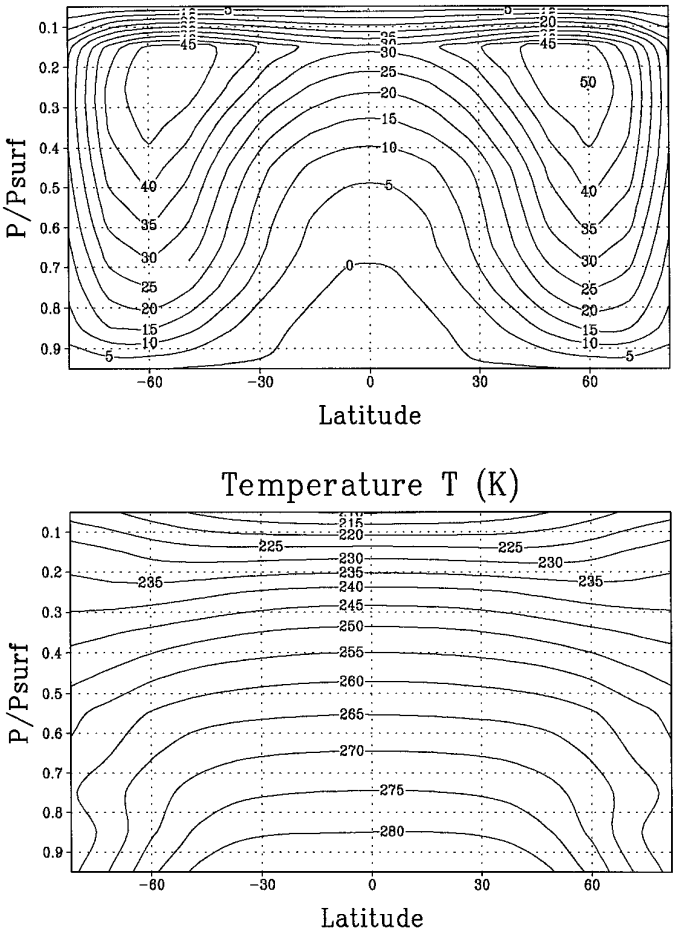

FIG. 1. Zonal wind u (m sec^{-1}) (top) and temperature (K) (bottom) in the control run (zonally symmetric heating and Titan's rotation rate).

The zonally averaged temperature displays the familiar pattern of relatively warm tropics and relatively cold poles, although there is no meridional temperature gradient at the ground equatorward of 40°. This is because the Hadley circulation extends into the midlatitudes and reduces these gradients, as seen in previous work (Del Genio *et al.* 1993). The ability of the SGCM to reproduce earlier results shows that it is a valid tool for use in simulating the circulations of slowly rotating planets.

Simulations with Synchronous Heating: Meridional Structure

We now examine the circulation in the standard 1000-mb run with synchronous heating present [see Eqs. (2) and (3)], denoted run 1 (Table I summarizes the runs). Plots of zonally averaged temperature and wind are shown in Fig. 2. The temperature exhibits an inversion at low levels. This is a consequence of averaging temperatures that vary a great deal over a line of latitude, as is shown in Fig. 3.

TABLE I
Run Summaries

Run	Pressure (mb)	τ	Radius (km)	Gravity (m sec^{-2})
1	1000	1.0	6400	9.8
2	100	0.25	6400	9.8
3	1500	1.5	6400	9.8
4	1000	0.25	6400	9.8
5	1000	0.5	6400	9.8
6	1000	2.0	6400	9.8
R1	1000	1.0	13000	9.8
R2	1000	1.0	13000	30
R3	1000	1.0	3400	3.72

Aloft, temperatures at the substellar and antistellar points are similar, but they are very different near the ground. There is a strong inversion at the antistellar point near the ground. This is due to small sensible heat transport be-

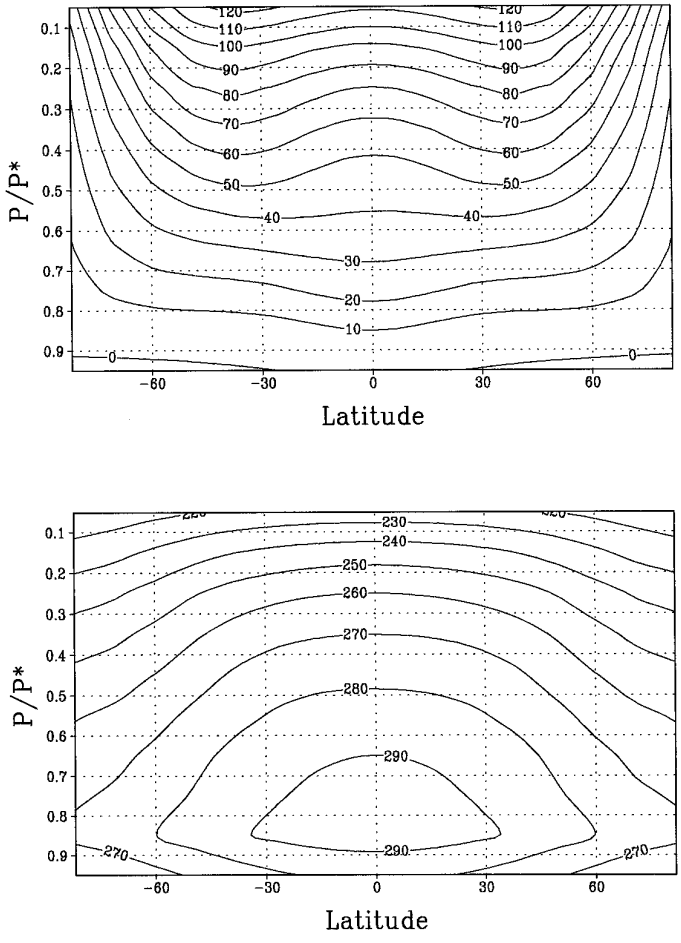

FIG. 2. Zonal wind u (m sec^{-1}) (top) and temperature (K) (bottom) in run 1. This is the standard run with synchronous heating present, a surface pressure of 1 bar, and terrestrial insolation.

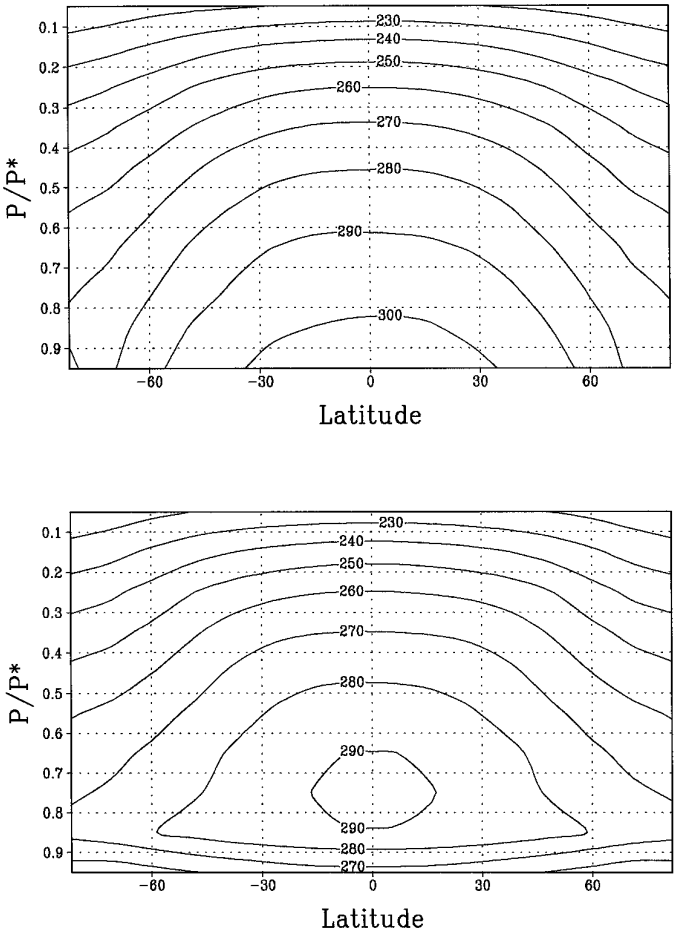

FIG. 3. Temperature (K) at the substellar point (top) and the antistellar point (bottom) in run 1. Note the strong inversion in the bottom figure.

tween ground and atmosphere because of the relatively statically stable conditions there.

The zonal wind pattern is dominated by a strong superrotation at high altitudes above the equator. To establish what mechanisms might be causing this pattern, the momentum fluxes from different mechanisms are now examined.

The horizontal and vertical eddy momentum fluxes are shown in Figs. 4 and 5, respectively. In each figure the contribution to the total momentum fluxes by transient and stationary waves is shown. The period used for obtaining the steady-state data was 20 Titan days (about 320 terrestrial days). The transient eddies cause significant equatorward momentum fluxes in the midlatitudes, which is typical of barotropic waves. The stationary eddies cause equatorward momentum transport at low levels, with large upward fluxes at the equator. This pattern is consistent with that thought to be important in setting up equatorial superrotating winds in planetary atmospheres (Gierasch 1975).

The stationary wave activity is associated with the thermal tide caused by the synchronous heating. This tide is the difference between run 1 and the control run shown above and, therefore, appears to be the crucial factor in setting up the strong equatorial superrotation. The momentum fluxes associated with this strong tide act to amplify the superrotation in the same way as the thermal tide on Venus is thought to amplify the superrotation there (Pechmann and Ingersoll 1984). In this case, however, the amplitude of the tide is much larger than on Venus, and results in very strong westerly winds at the model top.

The mean momentum fluxes associated with the zonally averaged circulation are shown in Fig. 6. There are large upward and poleward fluxes at high levels at the equator, consistent with divergence in this location associated with a zonally symmetric Hadley circulation (Gierasch 1975). However, nearer the poles, a more complex structure ex-

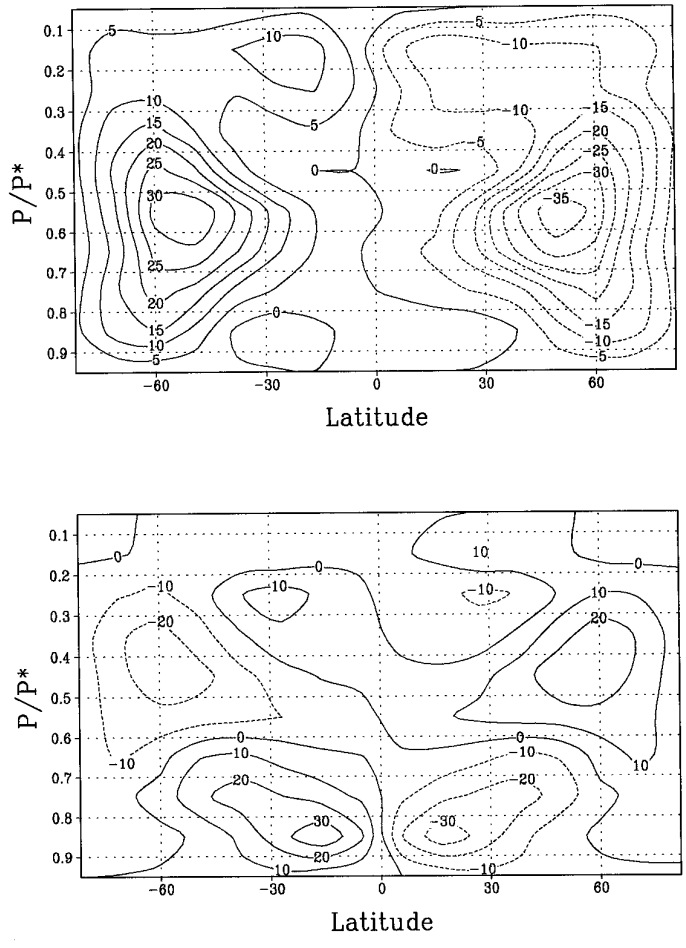

FIG. 4. Horizontal eddy momentum flux $\overline{u'v'}$ ($m^2 sec^{-2}$) contributions from transient waves (top) and stationary waves (bottom) in run 1. Positive values indicate a northward direction, so that there is net equatorial transport of momentum in the top figure. The bulk of the stationary wave activity results from the synchronous heating.

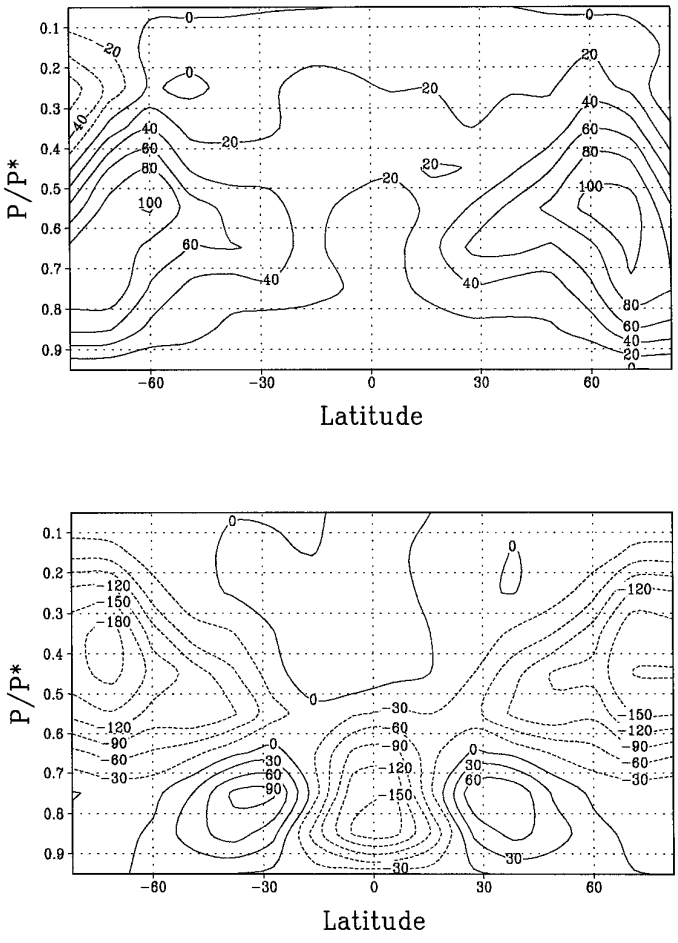

FIG. 5. Vertical eddy momentum flux $\overline{u'\omega'}$ [(m sec^{-1})(10^{-6} mb sec^{-1})] contributions from transient waves (top) and stationary waves (bottom) in run 1. Positive values indicate a downward direction. The bulk of the stationary wave activity results from the synchronous heating.

ists, with equatorward momentum fluxes at mid-levels in the subtropics followed by poleward fluxes at midlatitudes.

This structure can be explained by examining the zonally symmetric streamlines, which is shown in Fig. 7. This shows mean upward motion at the equator, balanced by downwelling near the poles but each hemispheric cell has a double center. This should be contrasted with Fig. 7 (bottom), taken from the control run, which exhibits the more familiar two cells extending from equator to midlatitudes. The double-cell pattern is reminiscent of that seen in simulations of the venusian atmosphere with an optically thick cloud present (Del Genio *et al.* 1993). The structure must be an artifact of the zonal asymmetry evident from Fig. 3.

Simulations with Synchronous Heating: Three-Dimensional Structure

Since a major component of the circulation is three-dimensional, looking at zonal averages of model diagnostics can only give a limited picture of the circulation. We now examine the three-dimensional circulation.

A longitudinal section of temperature in run 1 is shown in Fig. 8 (top). This shows the large thermal contrast between the low-level temperatures at the substellar point (at 0°W) and at the antistellar point (at 180°W). The effect of horizontal advection of heat from dayside to nightside can be seen by comparing this figure with Fig. 8 (bottom), which shows radiative equilibrium temperature for the standard 1-bar case (this latter run was performed by running the SGCM with the dynamics turned off). Heat advection transfers heat to the nightside, significantly warming it, especially at upper levels. A large inversion is present on the nightside at low levels in Fig. 8 (top). The lapse rate over most of the atmosphere is about 2 K km^{-1}, which is far removed from its adiabatic value of about 7 K km^{-1}, also indicative of the strong upward fluxes of heat by atmospheric motions.

Longitudinal sections of zonal wind u and ω (vertical

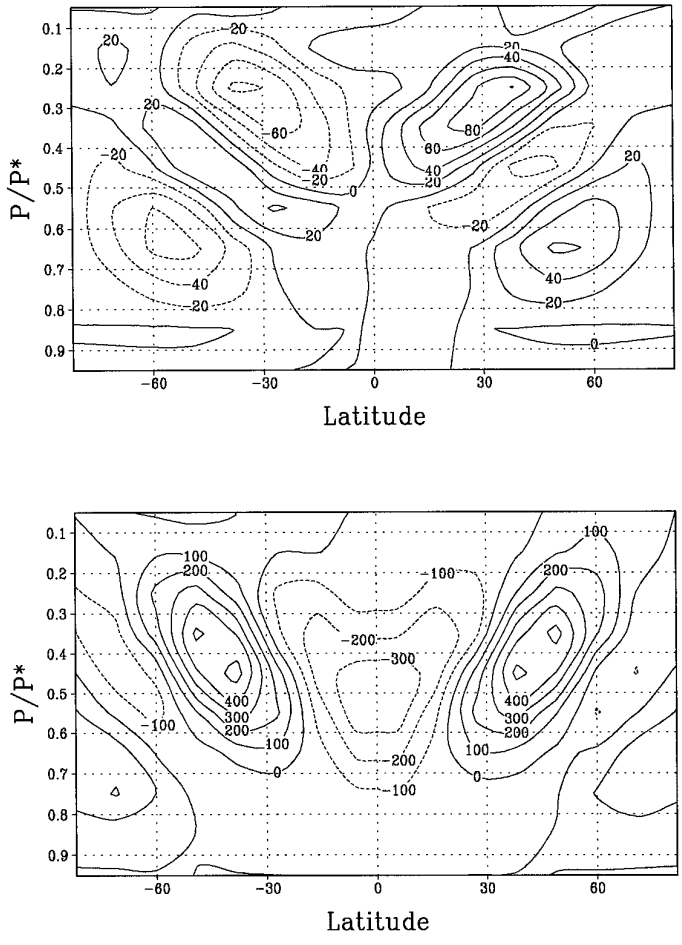

FIG. 6. Vertical mean momentum flux $\overline{u\omega}$ [(m sec^{-1})(10^{-6} mb sec^{-1})] (top) and horizontal mean momentum flux $\overline{uv}$ (m^2 sec^{-2}) (bottom) in run 1.

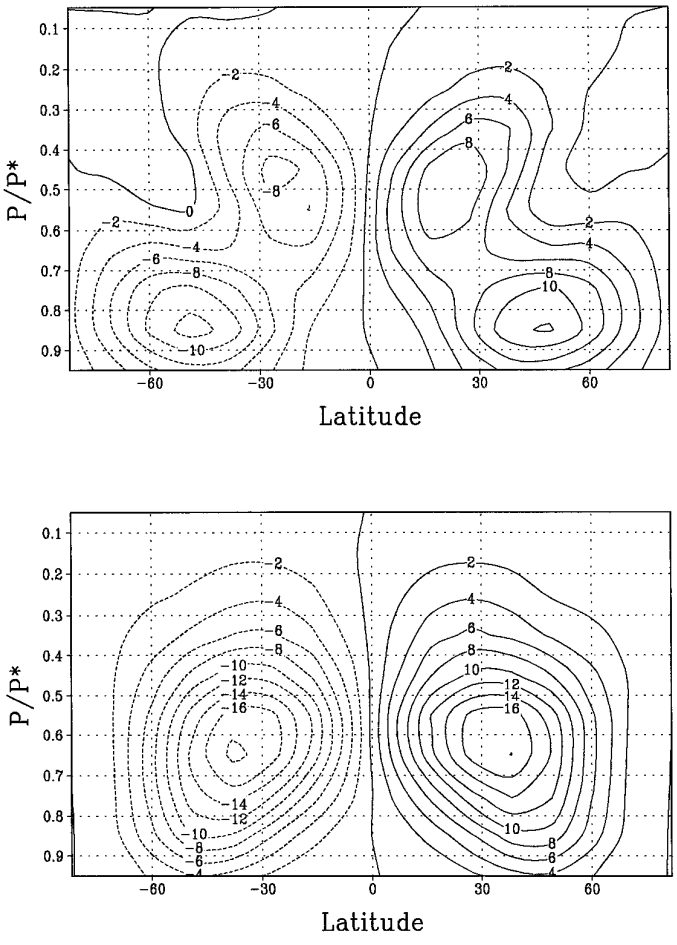

FIG. 7. Zonally averaged mean meridional circulation (kg sec^{-1} * 10^{10}) in run 1 (top) and the control run (bottom). The positive contours indicate clockwise motion on the diagram.

velocity in pressure coordinates) are shown in Fig. 9. The upward motion can be seen over the substellar point, with descending motion over the nightside. The strong superrotation is also seen, becoming more zonally symmetric as altitude increases. The vertical velocity ω exhibits a double peak, rather than one maximum above the subsolar point. Normally, upward mass flow is balanced by inflow of mass at low levels. However, as seen from Fig. 10, this does not happen. There is not enough mass flow into the substellar point to balance high vertical velocities there. Instead, the highest values of ω are found nearer the terminator.

The horizontal component of the circulation is shown in Figs. 10 and 11. Aloft, Fig. 11 shows a broad westerly jet with surprisingly little zonal variation compared with nearer the surface. Near the surface, mass (and heat) flows away from the substellar point both east and west at the equator, and returns through the polar regions.

The three-dimensional nature of the circulation is at first sight somewhat strange. One might expect the longitudinal component of the circulation to behave somewhat like a terrestrial-type Walker circulation, with rising motion over the dayside, flow toward the nightside at upper levels, which is returned to the dayside at lower level. This actually does happen, but along a great circle stretching from the substellar point, through the pole, to the antistellar point. Here, fluid flows at high levels across the pole from dayside to nightside, and is returned to the dayside at low levels across the pole, as shown in Fig. 12. This shows the eddy component of the wind vectors. The zonal average has been removed to isolate net transport. The flow across the polar region can be seen clearly in this case.

Elsewhere, this sort of thermally direct cell is disrupted by the strong zonal flow. Fluid can only flow across the terminator from dayside to nightside at low levels. Once on the darkside, since static stability is relatively high, vertical motion is subdued, and fluid can only return to the dayside at low levels through the thermally direct polar cell.

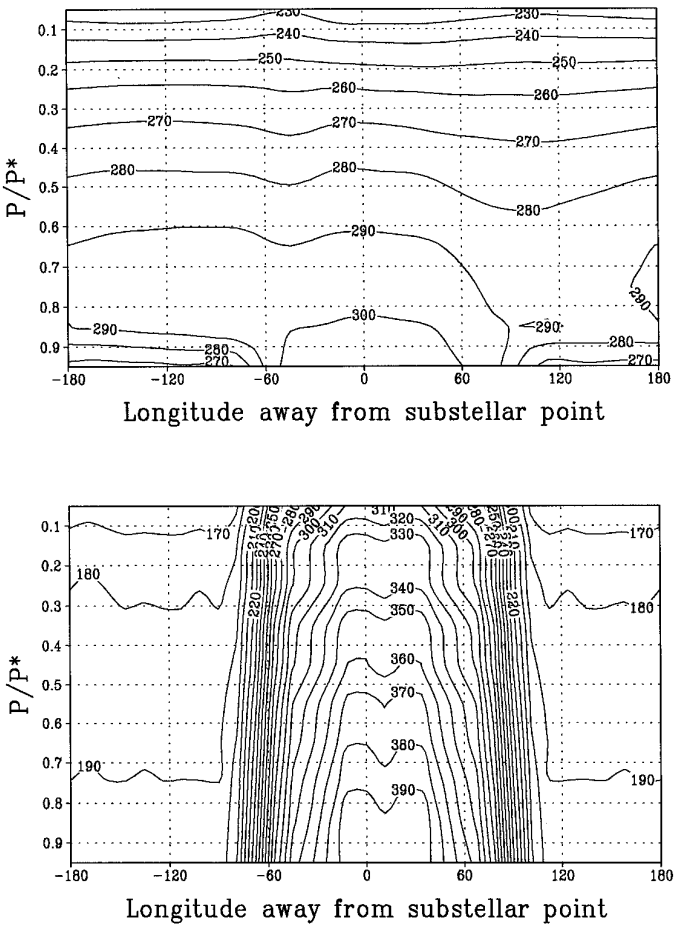

FIG. 8. Longitude–height section of temperature (K) at the equator in run 1 (top) and radiative equilibrium temperature (K) (bottom). Note that the bottom plot is not a steady state as CO_2 is able to condense on the darkside, but is merely shown as a comparison with the top plot.

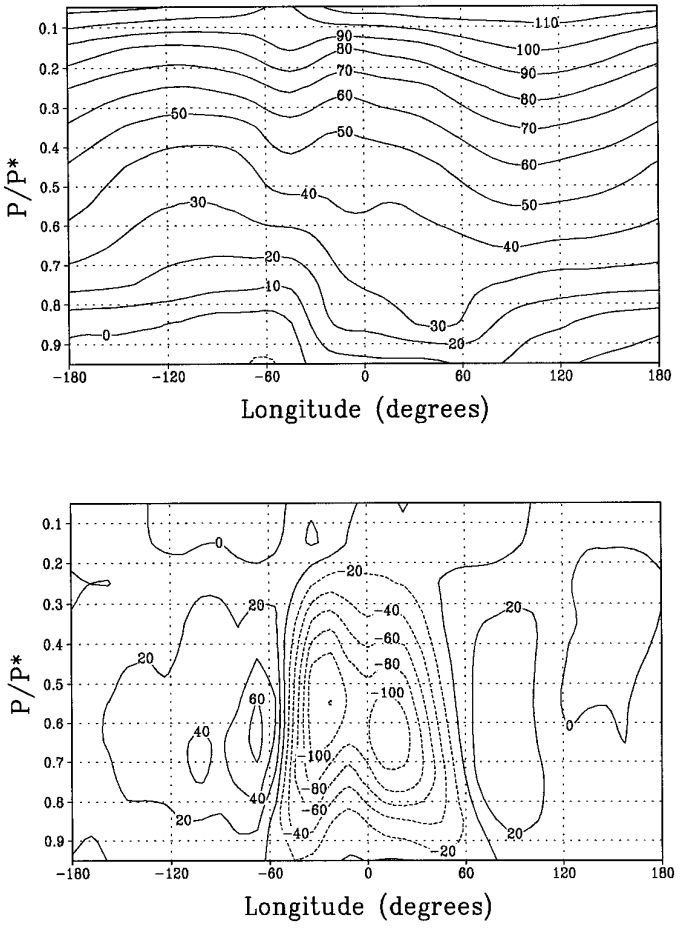

FIG. 9. Longitude–height section of u (m sec^{-1}) at the equator (top) and dp/dt (10^{-6} mb sec^{-1}) (bottom).

Transient Variations

Slowly rotating atmospheres can be barotropically and inertially unstable, due to the high wind shear present. Such instabilities manifest themselves as atmospheric waves, which have a very important role to play in maintaining the time–mean wind structure (Del Genio *et al.* 1993).

These disturbances manifest themselves in fields such as windspeed and T_0. Time series of these fields at the equator are shown in Fig. 13. A strong oscillation of period ≈1.5 Titan days can be observed, especially in the surface temperature. The amplitude in this latter quantity is 3–4 K, and is a signature of the barotropic instability discussed above. It must be emphasized that the period and amplitude of this oscillation are particular to this particular set of model parameters. Nevertheless, it should be noted that for reasonable model parameters, and for a surface whose thermal response time is $O(10^5$ sec), the surface can react to atmospheric variability with oscillations of amplitude O(a few K). This has implications for planetary habitability, as is discussed below.

One major cause of transience in planets orbiting M stars will be starspots. These are similar to those seen on the Sun, but are much larger in scale, causing a decrease in S of 10–40% and lasting for up to a few Earth months (Rodonò 1986). The ability of the atmosphere to respond to these changes is dependent on its thermal inertia, as well as the thermal inertia of the ground. While a precise prediction of temperature perturbations for a range of different starspots and atmospheric or surface properties is not feasible, a qualitative analysis of the spatial variation in atmospheric response to a typical starspot is feasible.

Again, the standard run 1 was repeated. The starspot was represented by a Gaussian perturbation to the stellar insolation of the form

$$S = S_0 - S_s \exp\left(-\left(\frac{t - t_{mean}}{t_\sigma}\right)^2\right), \qquad (6)$$

where S_0 was the nominal insolation, S_s was set in this case to 0.4 S_0 (a rather extreme value), t was time in Titan days, t_{mean} was the midpoint of the perturbation, set at 80 Titan

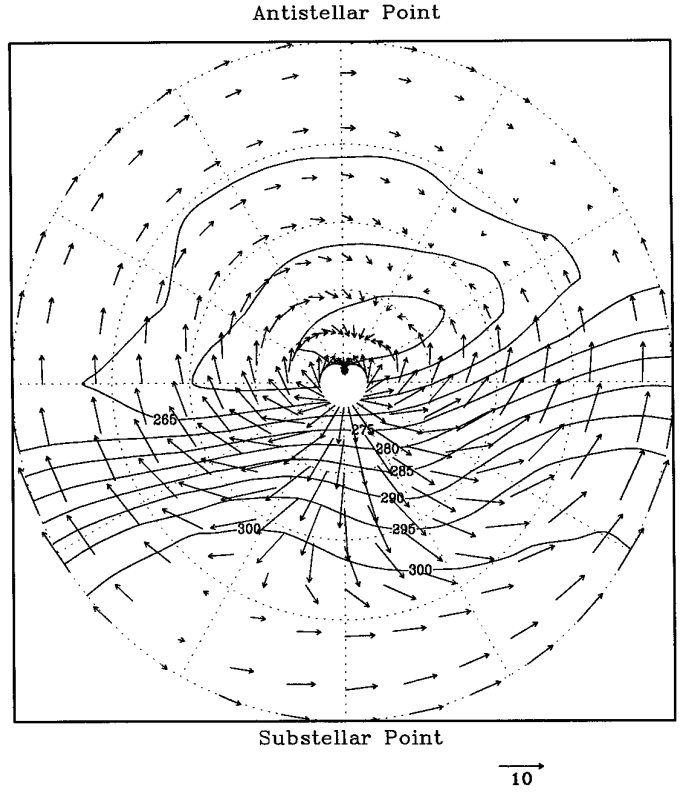

FIG. 10. Polar stereographic plot of temperatures (K) the horizontal wind vectors on the 950-mb surface (approximately 500 m above the ground).

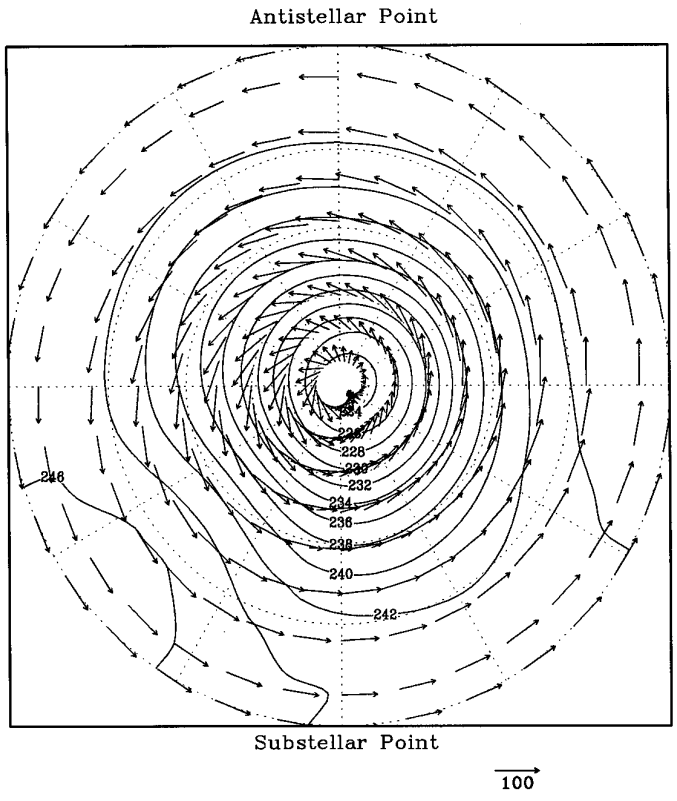

FIG. 11. Polar stereographic plot of temperatures (K) and horizontal wind vectors on the 150-mb surface (approximately 20 km above the ground).

days into the model integration, and t_σ was set to 2.0, so that the total duration of the starspot was 8 Titan days, or about 4 Earth months. This amplitude and duration were selected so that the atmosphere would have time to respond to an extremely large starspot, and the signal should be very large. Note the negative sign in Eq. (6), as starspots tend to reduce stellar brightness.

The surface temperature was analyzed at the substellar point, the antistellar point, and the eastern equatorial terminator, and is shown in Fig. 14. The largest response is at the substellar point, with the terminator and antistellar points responding on similar time scales, but with smaller amplitudes. As a comparison, if the planet was in radiative equilibrium, a 40% decrease in S would result in a 40 K decrease in T_0 at the substellar point, with the darkside being unaffected. The difference between these values and those in Fig. 14 is due to advection of heat by the atmosphere.

The substellar point reaches its minimum temperature 20 Earth days after the minimum in stellar brightness, due to the thermal inertia of the atmosphere/surface system. It takes almost twice as long for darkside temperatures to bottom out. By Earth day 64 after the starspot minimum,

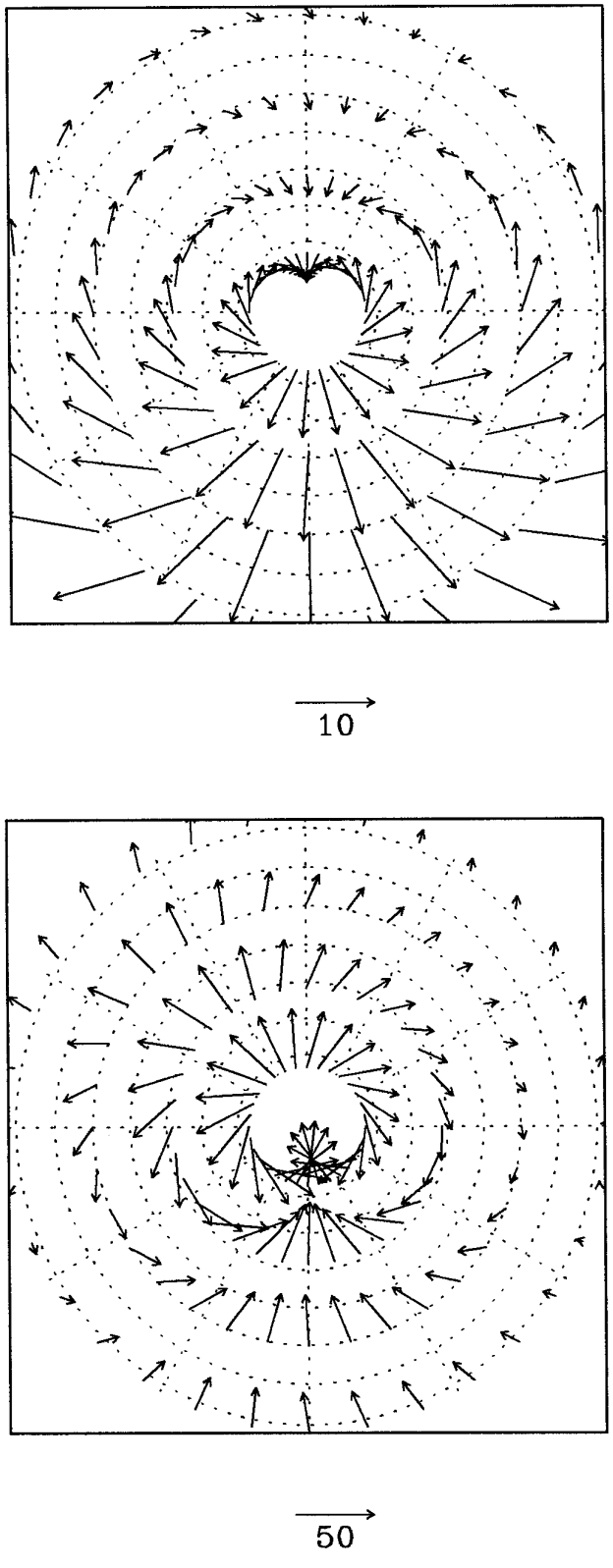

FIG. 12. Magnified polar stereographic plots of horizontal wind vectors on the 950-mb surface (top) and the 150-mb surface (bottom). The plot limits are 50°N to 90°N and zonal wind u vectors have had the zonal mean removed. Note the different scales for the wind vectors.

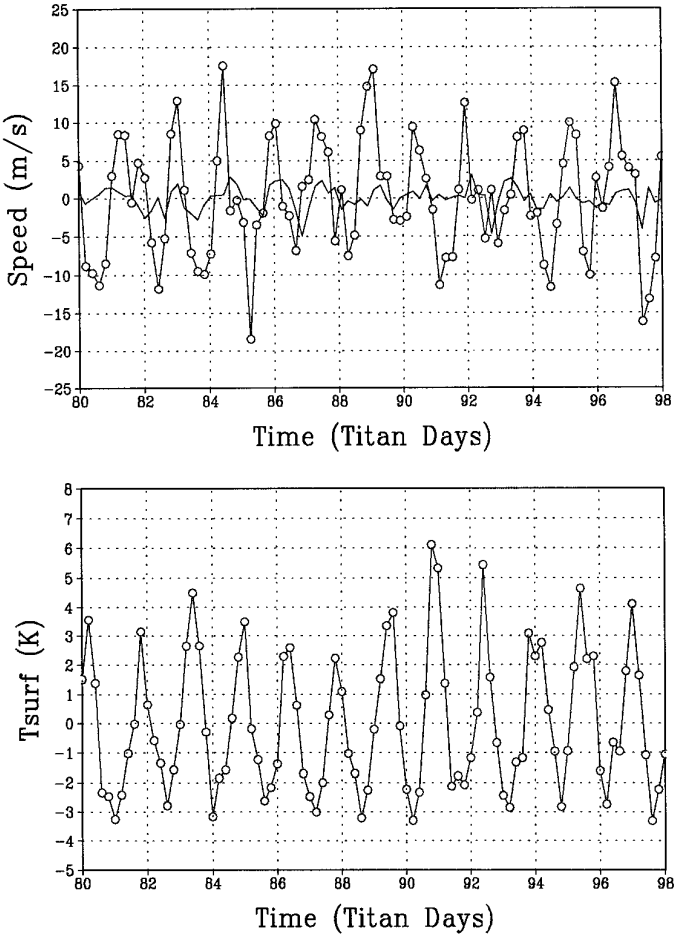

FIG. 13. Transient variability in the model in run 1 as shown by the wind speed (m sec^{-1}) at $\sigma = 0.95$ (top, unmarked) and at $\sigma = 0.25$ (top, circles), and by T_0 (K) (bottom). Each time series is taken at 63°E, 0°N (the equatorial terminator) and has had its time average removed.

S has returned to the nominal level, but T_0 takes twice as long to return to its pre-starspot level. The effect that this phenomenon might have on atmospheric collapse is considered below.

Other sources of transient variations would be brightness variations caused by non-zero orbital eccentricities. In the case of synchronously rotating planets, this would amount to a stationary thermal tide with a period equal to the rotation period and an amplitude dependent on the orbital eccentricity.

The response of T_0 to this phenomenon will depend on the rotation period (as this is the period of the variation of insolation) and the thermal inertia of the planet's atmosphere and surface. Atmospheres on planets orbiting larger M stars (having masses $\approx 0.5M_{\text{sun}}$) exhibit lower rotation rates and will therefore be able to respond more efficiently to variations in insolation induced by eccentricity.

SENSITIVITY STUDIES

The sensitivity of the SGCM to diabatic and external parameters is now investigated, with special detail given to how changes in these parameters affect surface temperatures.

Effect of Surface Pressure p_0

Figure 15 shows T_0 at the equator in three runs with different surface pressures. Run 2 exhibits the highest value of ΔT_{DN} (160 K), consistent with it being nearest to radiative equilibrium. While the darkside is at 200 K in this run, it is still above the freezing point of CO_2 at this pressure, indicating that even a 100-mb CO_2/H_2O-type atmosphere can transport enough heat to its darkside to prevent atmospheric collapse. Run 3 exhibits darkside temperatures that are high enough to support liquid water.

When the nominal runs were repeated for lower pressures, collapse was found to occur at a value of p_0 of approximately 30 mb. One reason why this surface pressure

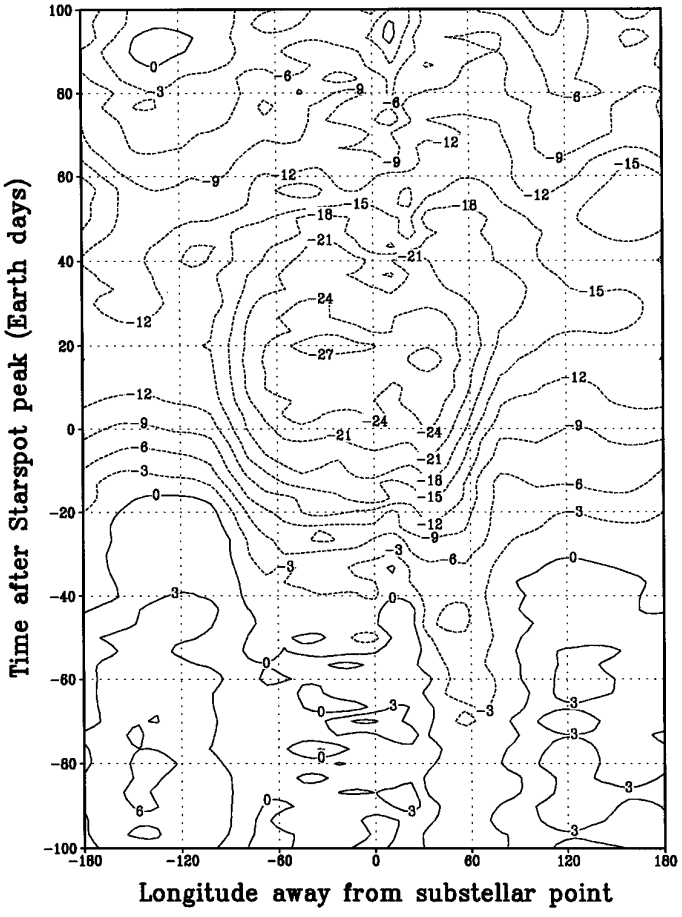

FIG. 14. T_0 at the substellar point. The values plotted have had the pre-starspot T_0 subtracted from them.

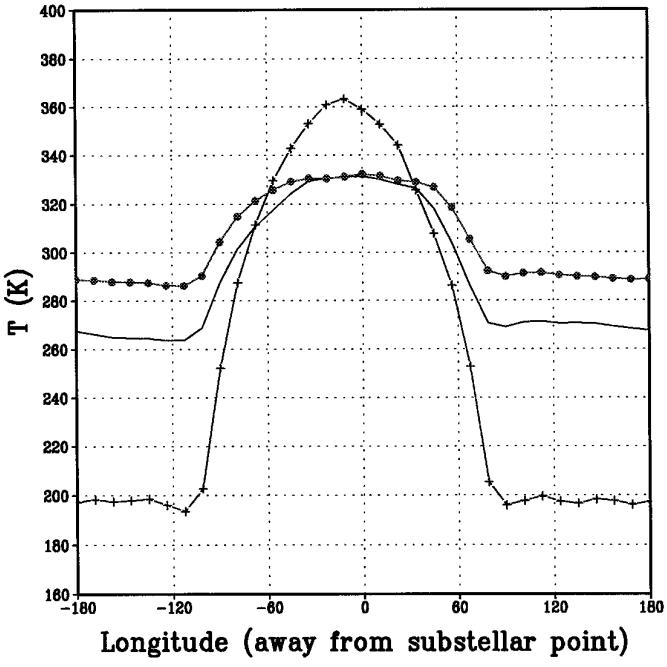

FIG. 15. Longitudinal sections of surface temperature (K) at the equator for runs with varying surface pressure: 1000 mb (unmarked), 100 mb (crosses), 1500 mb (circles).

is so low is that as pressure decreases, the frost point temperature T_c also decreases. T_c(1000 mb) is about 195 K, whereas T_c(30 mb) is approximately 160 K. Thus, even though less heat transport takes place in the latter run, T_0 on the darkside of the planet only barely reaches the frost point.

Haberle *et al.* (1996) predicted that 150 mb of CO_2 was necessary to prevent atmospheric collapse. Their result, while not in agreement with the SGCM, is correct to within an order of magnitude. One reason why their work may have overestimated the critical surface pressure is that their parameterization of heat transport was based on heat fluxes by baroclinic waves in terrestrial midlatitudes. As shown earlier, heat transport in the SGCM is accomplished by a vigorous thermally direct cell and strong zonal winds at low latitudes. Heat transport by this method is more efficient than transport by baroclinic waves, therefore lowering the pressure at which transport prevents atmospheric collapse.

The large ΔT_{DN} in run 2 is associated with a more vigorous circulation in the atmosphere. In run 2, u reaches well over 100 m sec^{-1} aloft. Lower down, winds exceed 20 m sec^{-1} (about 40 mph). The overall circulation pattern of zonal mass flow away from the substellar point, returning via the poles, and strong superrotation aloft, is the same.

Atmospheric temperatures, especially on the dark side, are far warmer than simple one-dimensional calculations suggest. This implies that the globally averaged value of T_0 must be colder than one-dimensional calculations suggest to conserve energy. This is in fact the case, as shown in Table II. The analytical values calculated are simply those calculated by $T_0^4 = (1 - a)(1 + \tau)F/\sigma$. In each case, T_0 in the model is about 30 K colder than the one-dimensional results. It is only at the subsolar point that temperatures exceed the one-dimensional values, as it is here that the lapse rate is nearest the radiative profile. This was noted to a certain extent by Kasting *et al.* (1993), who pointed out that a one-dimensional radiative–convective model would give only a maximum limit on the planetary mean T_0. However, the magnitude of the difference is such that it should be noted when using one-dimensional calculations to calculate habitable zone limits.

TABLE II
Mean T_0: Analytical and Model Results

	T_0 (K)	
Run	Analytical	Model
1	313.4	285.5
2	278.7	247.9
3	331.4	299.3

At high surface pressures, the SGCM results should asymptote to the one-dimensional results. This is because ΔT_{DN} tends to zero, and so the effect of atmospheric temperatures being warmer than one-dimensional radiative calculations (see Table II) is minimized. This gives further weight to the assumption that the SGCM only provides a significant improvement in predicting habitable zone boundaries over one-dimensional simulations for pressures lower than approximately a few bars. At pressures above these, the inaccuracies in the gray radiation scheme outweigh the advantages gained by simulating the finite ΔT_{DN}.

Effect of Radiation Parameters

The prescription of optical depth with pressure is now relaxed to examine the effect of different atmospheric compositions. For instance, a thick N_2 atmosphere with trace amounts of CO_2 will have a p_0 value of O(bars), but a very small value of τ (although it should be noted that the Earth, having a mainly N_2 atmosphere with a greenhouse effect coming mainly from H_2O, does have a gray IR optical depth of about 0.9).

The optical depth should not change the radiative time scale t_r to first order, as changing τ does not dramatically change T_e. However, increasing τ will increase T_0, and hence drive a more vigorous circulation, which should act to lower ΔT_{DN}. The effect of changing τ at a given pressure

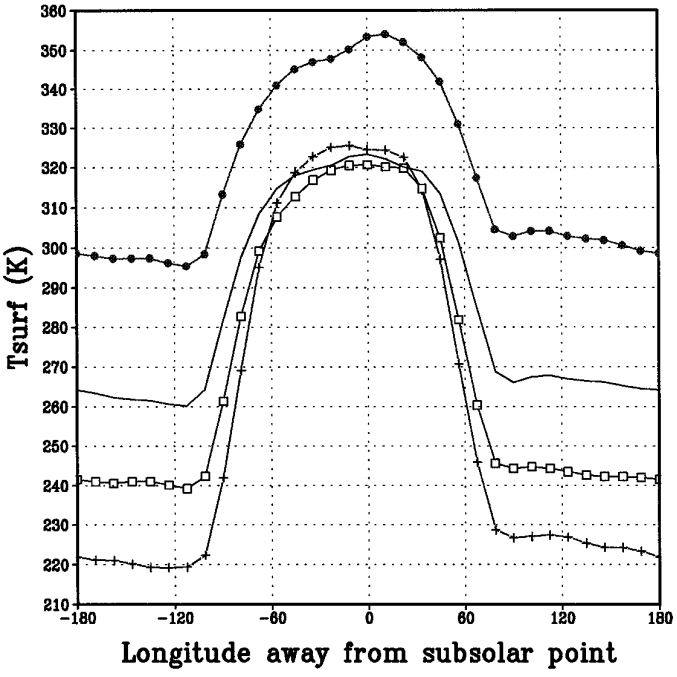

FIG. 16. T_0 in runs 1, 4, 5, and 6. Run 1 ($\tau = 1$, unmarked); run 4 ($\tau = 0.25$, crosses); run 5 ($\tau = 0.5$, squares); run 6 ($\tau = 2.0$, filled circles).

was examined by doing three more runs, denoted runs 4, 5, and 6 (see Table I). T_0 and ΔT_{DN} in these runs were then compared with run 1.

Figure 16 shows T_0 in runs 1, 4, 5, and 6. As is expected, the average value of T_0 increases with τ. However, ΔT_{DN} decreases dramatically as τ increases. As τ increases from 0.25 to 1.0, darkside temperatures rise by almost 80 K, whereas subsolar point temperatures actually fall between runs 4 and 5 before rising again. Only when τ increases to 2 in run 6 do the subsolar point temperatures start to increase in tandem with the antistellar point temperatures.

These results indicate that T_0 at the substellar point is insensitive to τ at low optical depths. Only in optically thick atmospheres ($\tau > 1$) is the substellar point surface temperature affected strongly by the greenhouse effect. This hypothesis was tested by rerunning run 2, but with optical depths of 1.0 and 2.0. In these experiments, the substellar T_0 increased steadily from 360 to 400 K. IR optical depth therefore seems to affect ΔT_{DN} only at pressures of O(1000 mb). This is probably because only at these higher pressures is heat transport the most important factor in determining T_0, and thus only at these higher pressures can the feedback of τ onto the heat transport significantly affect T_0.

Effect of External Parameters

Varying model parameters such as the coefficients governing drag and heat transfer between atmosphere and surface or radiation parameters such as surface albedo will obviously cause some change in the results obtained. For instance, higher coefficients for internal vertical diffusion will result in lighter winds. Quantitatively examining the model response to changes in each of these parameters is beyond the scope of this work. We therefore concern ourselves in this section only with those parameters that might cause fundamental changes in the circulation regime seen in the model.

Rotation rate ω is one such parameter, since, as stated earlier, it fundamentally affects the circulation regime in which the planet lies. Run 1 was repeated, but with two different values of ω: 10^{-6} and 10^{-5} sec^{-1}. These are the expected minimum and maximum values derived in an earlier section. In each case surface temperatures matched those in run 1 to within 5 K, and $\bar{u}$, the zonally averaged zonal wind, displayed a pattern of westerlies over the equator. The strength of the zonal wind at the equator actually increased slightly with ω. At low levels, fluid flowed away from the substellar point at the equator, and returned via the poles, as in run 1. The relative insensitivity of the results to rotation rate is an indication that the synchronous heating is dominating the SGCM response. Without it, flow patterns are strongly sensitive to ω (James 1994).

The effect of planetary size was considered. ΔT_{DN} is dependent on a balance between radiation and advection, and advective heating is given by $u\nabla T$, so doubling the radius of the planet should decrease ∇T, and hence increase ΔT_{DN}. However, increasing g will also decrease the radiative relaxation time [see Eq. (1)], and increase the adiabatic lapse rate, and hence change T_0 in a nontrivial fashion. The effect of this was examined by performing two runs with planetary radius set to 13×10^6 m. One was done with g held at 9.8 m sec^{-2} (run R1) and one in which $g =$ 30 m sec^{-2} (run R2). The reason for this was to separate the effect of the large radius and the combined effect of the large radius and a higher g.

The results are shown in Fig. 17. Run R1 exhibited surface temperatures slightly higher than those of run 1, although the change was only about a maximum of ± 10 K. Run R2 exhibited far greater differences, consistent with the lower radiative relaxation time due to a higher value of g. The substellar lapse rate was also higher in R2, with the model top being 10 K colder than the control run. This result indicates that the change in parameters such as g associated with a change in planetary mass is more important than the actual planetary size itself. The implications of this for habitability are discussed below.

Run 1 was again repeated, but with radius and g set to martian values (run R3). As expected, ΔT_{DN} was reduced to 40 K, with T_0 on the nightside at 270 K. As stated earlier though, such planets are too small to continually recycle gases like CO_2 into their atmospheres (Carr 1981), and so one might expect such planets to have atmospheres similar

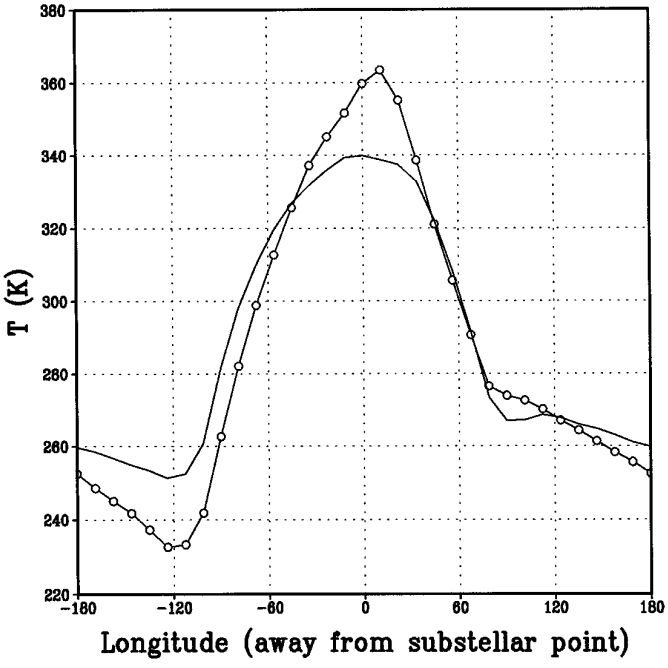

FIG. 17. Longitudinal sections of surface temperature (K) at the equator for the planetary radius = $2a_{\text{Earth}}$ runs with $g = g_{\text{Earth}}$ (unmarked) and $g = 3g_{\text{Earth}}$ (circles).

to that of Mars. Run R3 was repeated, but with different values of p_0, to check at what value a Mars-type planet ceased to support an atmosphere when $S = 1$. A permanent nightside cap formed when $p_0 \approx 10$ mb. This value is much lower than previously found. The reason for this is that the smaller planetary radius (and hence smaller advective time scale), as well as the smaller value of g, drives the atmosphere further away from radiative equilibrium than the case with terrestrial parameters. This results in a smaller ΔT_{DN} for a given surface pressure, and hence a lower pressure at which atmospheric collapse occurs.

HABITABILITY

Atmospheric Collapse

We now discuss the outer edges of habitable zones around M stars. The outer edge of such a zone will occur when a planetary atmosphere can no longer transport enough heat to its darkside to prevent collapse. One-dimensional calculations have shown that this happens when insolation $S = 0.27$ (Kasting *et al.* 1993). In the three-dimensional simulations, collapse occurs even when mean insolation is above this value, due to a finite ΔT_{DN}. Run 2 is very close to atmospheric collapse, despite having an insolation S of 1.

Run 1 was repeated with lower values of S to find out at which value of S the standard 1000-mb atmosphere collapsed. Reducing S reduces T_e, the temperature at the top of the atmosphere, which then increases the radiative time scale [see Eq. (1)]. This should then reduce ΔT_{DN}. For example, when run 1 was repeated with $S = 0.44$ (equal to martian insolation), $\Delta T_{\text{DN}} = 50$ K, which was about 70% of its value in run 1. Atmospheric collapse actually occurs at $S = 0.3$. This is slightly higher than the one-dimensional calculations suggest, again because of a finite ΔT_{DN}, but is nevertheless very close to the one-dimensional predictions.

We now note that the Kasting first condensation limit, defined as when CO_2 clouds first form (Kasting *et al.* 1993), does not apply to synchronous rotators. This is because large inversions form above the nightside surface as seen in Fig. 8. The lapse rate here is therefore very much more positive than that associated with CO_2 condensation, and CO_2 will therefore condense at the ground before it condenses in the atmosphere.

While the feedbacks associated with CO_2 condensation may not take place on these planets, feedbacks associated with large changes in S due to starspots may cause the atmospheres of such planets to collapse. Once this happens, the atmosphere may not be able to revert to its original state when the stellar brightness increases again. This is because in the collapsed state, p_0 is O(mb) [cf. martian permanent polar caps (Toon *et al.* 1980)], which is below the minimum CO_2 pressure needed to support an atmosphere when $S = 1$. However, as shown in Fig. 14, if the surface pressure is sufficiently high, the darkside will experience a far smaller change in T_0 than purely radiative considerations suggest. In addition, results from SGCM simulations in which atmospheric collapse actually takes place suggest that the time scale for condensing a bar of CO_2 is O(years) rather than O(months). Thus, a high-amplitude starspot lasting for months should only result in condensation of a few percent of atmospheric mass before reevaporation takes place. We therefore conclude that starspots should play a role in atmospheric collapse only if p_0 is O(100 mb) or less.

Different atmospheric constituents will display different condensation temperature/pressure relationships. This will affect the minimum bound of p_0 at which atmospheric collapse occurs. For instance, an N_2 atmosphere will collapse when the darkside falls below the freezing point of N_2, which is about 80 K. Since even in runs 2 and 4 (both runs in which optical depth τ is very low) T_0 on the darkside does not even approach this value, it appears that synchronously rotating planets are able sustain N_2-type atmospheres having very low optical depths.

Habitable Zone Limits

Planets orbiting M stars will face constraints on habitability that occur because of the special characteristics that these stars have. One stellar phenomenon that could dramatically hinder habitability is flaring. M stars experience

flares that are relatively large in magnitude when compared with G stars (Rodonò 1986). Heath *et al.* (1996) have shown that organisms may be able to adapt to the effects of flares. However, this is one area where further research is necessary.

The stellar terminator on a synchronously rotating planet is a fixed location, and this location, while receiving some stellar insolation at all times, will never experience the full magnitude of a flare. The phenomenon of tidal locking will therefore help to mitigate the effects of stellar flaring at some locations such as the terminator, while amplifying the effects of flares at other places such as the substellar point.

Kasting *et al.* (1993) defined the inner edge of the habitable zone as when the stratosphere of a planet becomes saturated. At this point, hydrogen loss rates at the exobase become large, and water is lost quickly from the planet. However, since M stars are relatively cool, they radiate very little energy in bands shorter than 0.2 μm, leading to rates of H_2O breakdown that are so low that water loss may not be an issue (Heath *et al.* 1996).

While this is one area where further one-dimensional climate modeling is needed to quantify water loss rates, the finite ΔT_{DN} associated with synchronous rotation of planets orbiting M stars must then be taken into account in these calculations. As shown in Fig. 15, if the surface pressure of a synchronous rotator is low, ΔT_{DN} is high and the darkside T_0 will be very low, making the darkside a very efficient water trap (see, e.g., Fig. 15). The globally averaged water vapor concentration in such an atmosphere might then be expected to be far lower than purely one-dimensional calculations might suggest. The presence of a global ocean acting to recycle water across hemispheres would negate this effect, as it does on Earth.

If a water trap does occur on the darkside, the inner edge of the habitable zone for planetary atmospheres that have low surface pressures might then therefore be defined as that value of S where temperatures approach the melting point of water on the darkside. At this point liquid water can flow into the dayside and evaporate, and loss rates increase. In the SGCM, with p_0 set to 100 mb, this limit occurs when $S \approx 3$. Of course, at this insolation T_0 at the substellar point would reach unbearably hot temperatures (almost 500 K), and only the darkside and the terminator would be able to support any life.

Water loss at the inner edge of the habitable zone on large planets should take place at higher values of S than it does for Earth-sized planets, as the higher gravity on the large planets makes hydrodynamic escape more difficult. However, climate collapse on large planets will take place at higher values of S than on Earth-sized planets, due to the higher ΔT_{DN} on these large planets. The edges of the habitable zone therefore move upward in S as planetary radius increases.

We now translate the habitable zone limits from S coordinates into distances from an M0 star for the 1000- and 100-mb runs. The habitable zone will be approximately in the range $0.25 < h < 0.45$ (where h is in AU) if $p_0 = 1000$ mb and $0.14 < h < 0.3$ if $p_0 = 100$ mb. These values are of course dependent on factors such as optical depth τ and planetary radius g, as the above sensitivity studies show. The values obtained should be compared with the fixed value of $0.25 < h < 0.47$ (Kasting *et al.* 1993).

The above habitable zone limits all assume that atmospheric collapse occurs when CO_2 freezes out. It should be pointed out that greenhouse gases such as CO_2 and H_2O may only form minor constituents in an atmosphere consisting mainly of N_2 (such as the Earth). If this is the case, when the darkside falls below the frost point of CO_2, the atmosphere will be left with a very cold N_2 atmosphere with no greenhouse gases present. In this case, rather than being controlled by a combination of p_0 and τ, as is the case with no atmospheric condensation, surface temperatures will be set by p_0 and T_0 on the darkside, since this latter quantity is fixed near the CO_2 frost point.

Effects of Weathering

One factor that will affect the mean T_0 of a planetary atmosphere is CO_2 recycling. When liquid water is present, CO_2 will be recycled into carbonates, cooling the climate. If liquid water does not exist on the surface, the rate of carbonate formation decreases, and CO_2 can build up in the atmosphere, increasing its greenhouse effect and possibly even raising T_0 to the point where liquid water is once more stable (Kasting 1988).

This effect will act to raise p_0 to 1000–1500 mb of CO_2 at $S = 1$ and to higher pressures at lower values of S. Thus, if CO_2 partial pressure is controlled by the carbonate–silicate cycle, 1000–1500 mb of CO_2 will be the minimum surface pressure of a habitable synchronously rotating planet. If other greenhouse gases such as methane and ammonia exist in the atmosphere, this pressure limit will be lowered. The minimum p_0 of 1000–1500 mb will be higher if CO_2 is a minor component of an otherwise optically thin atmosphere or the surface albedo is higher. Clouds will also have an impact on this minimum p_0 value, depending on their optical properties.

It is beyond the scope of this paper to fully map out (S, p_0) space to produce a function relating p_{min} to S. This is because at low values of S, p_{min} would probably be O(bars), and, as previously stated, the one-dimensional model of Kasting *et al.* (1993) would calculate surface temperatures more accurately than the three-dimensional model.

The presence of the weathering cycle will depend on planetary size. If the planet is too small (e.g., run R3), volcanism ceases and CO_2 recycling stops, and this whole discussion is academic (Carr 1981). If the planet is too

large (e.g., run R2), the combination of higher advective heating time scales and higher gravity means that pressures and optical depths even higher than those discussed above will be needed to support liquid water on the surface at an insolation of $S = 1$.

CONCLUSIONS

We have modeled the circulation of atmospheres on terrestrial-type planets in potential habitable zones around M stars and find that such planets should be able to support atmospheres. For reasonable values of surface pressure they may even be able to support liquid water, at least for short periods and at certain times. Starspots, orbital eccentricity, and atmospheric variability can contribute to this transience.

The circulation of these planets consists of a longitudinal thermally direct cell which transports heat from the dayside to the nightside. This mass is returned to the dayside through the polar regions at low levels. Aloft the circulation is fairly longitudinally symmetric, and a superrotating jet is present at the equator as a consequence of the planet's slow rotation as well as the synchronous heating that it undergoes. Surface temperatures on these planets are well below those expected from radiative considerations, due to the atmosphere being far warmer than radiative–convective calculations suggest, especially on the nightside. Waves associated with the presence of surface features, such as spatially varying albedo and mountain ranges, might be expected to change the nature of the circulation aloft (Hourdin *et al.* 1995), but such work is beyond the scope of this paper. We merely note the possibility of such phenomena.

Habitable zones around M stars are not simply a function of stellar size. This is because habitable zones in these cases are determined by the temperature extrema that the planet's surface achieves. These extrema are in turn determined by factors such as atmospheric composition, pressure, and planetary size. The carbonate–silicate cycle will have a large impact on the minimum surface pressure that a habitable planet can sustain, by adding CO_2 to the atmosphere until darkside surface temperatures reach 273 K. Planetary size and mass also have a bearing on the habitable zone of such planets.

Further research using such a three-dimensional model might include quantifying the effects of heat transport by a global ocean. Other future work might concentrate on how the constituents of such atmospheres might evolve over geological time, given the small time-mean stellar UV fluxes, as well as the strong longitudinal asymmetry of this flux. The effect of basal melting of permanent darkside caps should be investigated too. The phase changes of constituents such as H_2O associated with transient warming and cooling events such as starspots might also be modeled more quantitatively.

M stars make up the majority of the population of main sequence stars (Rodonò 1986). In addition, modeling studies show that planets are able to form in the habitable zones of such stars (Wetherill 1996). Given these arguments, as well as the results presented above, we conclude that M stars should not be ruled out in the search for habitable planets.

ACKNOWLEDGMENTS

The authors thank Kevin Zahnle, Laurance Doyle, and Martin Heath for their useful feedback, as well as Michael Allison and Matthew Collins for their constructive comments as reviewers of this manuscript. Manoj Joshi is an associate of the U.S. National Research Council.

REFERENCES

Carr, M. H. 1981. *The Surface of Mars.* Yale Univ. Press, New Haven, CT.

Del Genio, A. D., and R. J. Suozzo 1987. A comparative study of rapidly and slowly rotating dynamical regimes in a terrestrial general circulation model. *J. Atmos. Sci.* **44,** 973–986.

Del Genio, A., W. Zhou, and T. Eichler 1993. Equatorial superrotation in a slowly rotating GCM: Implications for Titan and Venus. *Icarus* **101,** 1–17.

Dole, S. H. 1964. *Habitable Planets for Man.* Blaisdell, New York.

Gierasch, P. J. 1975. Meridional circulation and the maintenance of the Venus atmosphere rotation. *J. Atmos. Sci.* **32,** 1038–1044.

Goody, R. M., and Y. L. Yung 1989. *Atmospheric Radiation,* p. 447. Oxford Univ. Press, Oxford.

Haberle, R., C. McKay, D. Tyler, and R. Reynolds 1996. Can synchronously rotating planets support an atmosphere? In *Circumstellar Habitable Zones.* Travis House, Menlo Park, CA.

Haberle, R. M., J. Pollack, J. Barnes, R. Zurek, C. Leovy, J. Murphy, H. Lee, and J. Schaeffer 1993. Mars atmospheric dynamics as simulated by the NASA/Ames general circulation model. I. The zonal mean circulation. *J. Geophys. Res.* **98,** 3093–3124.

Heath, M. J., L. R. Doyle, R. M. Haberle, and M. M. Joshi 1996. Habitability of planets around red dwarf stars. *Origins Life,* submitted for publication.

Hide, R. 1969. Dynamics of the atmospheres of the major planets with an appendix on the viscous boundary layer at the rigid bounding surface of an electrically-conducting rotating fluid in the presence of a magnetic field. *J. Atmos. Sci.* **26,** 841–853.

Holton, J. R. 1992. *An Introduction to Dynamic Meteorology,* Ch. 2. Academic Press, San Diego.

Hoskins, B. J., and A. J. Simmons 1975. A multi-layer model and the semi-implicit method. *Q. J. R. Meteorol. Soc.* **101,** 637–655.

Hourdin, F., O. Talagrand, R. Sadourny, R. Courtin, D. Gautier, and C. P. McKay 1995. Numerical simulation of the general circulation of the atmosphere of Titan. *Icarus* **117,** 358–374.

James, I. N. 1994. *Introduction to Circulating Atmospheres.* Cambridge Univ. Press, Cambridge.

James, I. N., and Gray, L. J. 1986. Concerning the effect of surface drag on the circulation of a baroclinic planetary atmosphere. *Q. J. R. Meteorol. Soc.* **112,** 1231–1250.

Joshi, M. M., and Haberle, R. M. 1996. On the ability of synchronously rotating planets to support atmospheres. In *Astronomical and Biochemical Origins and the Search for Life in the Universe,* (C. B. Cosmovici, S. Bowyer, and D. Wertheimer, Eds.), pp. 351–359. Editrice Compository, Bologna, Italy.

Joshi, M. M., S. R. Lewis, P. L. Read, and D. C. Catling 1995. Western boundary currents in the martian atmosphere: Numerical simulations and observational evidence. *J. Geophys. Res.* **100,** 5485–5500.

Kasting, J. F. 1988. Runaway and moist greenhouse atmospheres and the evolution of Earth and Venus. *Icarus* **74,** 472–494.

Kasting, J. F. 1991. CO_2 condensation and the climate of early Mars. *Icarus* **94,** 1–13.

Kasting, J. F., D. P. Whitmire, and R. T. Reynolds 1993. Habitable zones around main sequence stars. *Icarus* **101,** 108–128.

Pechmann, J. B., and A. P. Ingersoll 1984. Thermal tides in the atmosphere of Venus: Comparison of model results with observations. *J. Atmos. Sci.* **41,** 3290–3313.

Pollack, J. B., J. F. Kasting, S. M. Richardson, and K. Poliakoff 1987. The case for a wet, warm climate on Mars. *Icarus* **71,** 203–224.

Rodonò, M. 1986. The atmospheres of M dwarfs: Observations. In *The M-Type Stars* (H. R. Johnson and F. R. Querci, Eds.), NASA SP-492, pp. 409–453. U.S. Govt. Printing Office, Washington, DC.

Toon, O. B., J. B. Pollack, W. Ward, J. A. Burns, and K. Bilski 1980. The astronomical theory of climate change on Mars. *Icarus* **44,** 552–607.

Wetherill, G. W. 1996. The formation and habitability of extra-solar planets. *Icarus* **119,** 219–238.

Williams, D. M., J. F. Kasting, and R. A. Wade 1996. Habitable moons around extrasolar giant planets. *Bull. Am. Astron. Soc.* **28,** 1115.

Yung, Y. L., and J. P. Pinto 1978. Primitive atmospheres and implications for the formation of channels on Mars. *Nature* **288,** 735–738.

Zahnle, K. J., and J. C. G. Walker 1982. The evolution of solar ultraviolet luminosity. *Rev. Geophys. Space Phys.* **20,** 280–292.